



Spectroscopy and catalytic activity study of gold supported on barium titanate nanotubes for styrene epoxidation

Devadutta Nepak^{a,b}, Darbha Srinivas^{a,b,*}

^a *Catalysis and Inorganic Chemistry Division, CSIR-National Chemical Laboratory, Pune 411 008, India*

^b *Academy of Scientific and Innovative Research (AcSIR), New Delhi 110 001, India*



ARTICLE INFO

Article history:

Received 14 April 2016

Received in revised form 10 May 2016

Accepted 16 May 2016

Available online 18 May 2016

Keywords:

Au nanoparticles

Titanate nanotubes

Styrene oxidation

Reactive oxygen species

Spectroscopy

ABSTRACT

Gold (0.5–5 wt.%) supported on barium titanate nanotubes (Au/BaTNT) were prepared, characterized and for the first time, investigated as catalysts for selective oxidation of styrene with oxygen (O_2 or $H_2 + O_2$) and peroxides (H_2O_2 or TBHP). Conversion of styrene enhanced when H_2 was co-added to O_2 in the reactions. Au/BaTNT activated O_2 and H_2 and produced H_2O_2 *in situ* for use in oxidations. Peroxides were found better oxidants than O_2 . At optimized conditions, styrene oxide selectivity of 80.1 wt.% at styrene conversion of 60.5 wt.% was achieved over Au(1 wt.%)/BaTNT using TBHP. Au particles (5.0–7.4 nm) were dispersed and decorated on the walls of BaTNT. They exhibited superior performance to the known Au catalysts in styrene oxidation. *Reactive oxygen species* formed during oxidation reactions were followed with *in situ* spectral characterizations (diffuse reflectance UV-vis and FT-Raman). Au/BaTNT was reusable in four recycles with little loss in catalytic activity.

© 2016 Elsevier B.V. All rights reserved.

1. Introduction

Selective oxidation of olefins (in particular, styrene) is an important chemical reaction as the products of this reaction (epoxide and aldehyde) are building units in the manufacture of plasticizers, perfumes and pharmaceuticals [1]. Epoxides are conventionally prepared by chlorohydrin/peracid routes, which are unsafe and generate a large quantity of waste with a heavy environmental burden with respect to its disposal. Use of molecular oxygen or a more reactive form of oxygen (H_2O_2 or *tert*-butyl hydroperoxide (TBHP)) as oxidant and metal as catalyst has been exploited as a *greener* approach for this reaction. However, epoxidation of olefins by the electrophilic addition of oxygen to the carbon–carbon double bond remains one of the most significant challenges in oxidation catalysis. There have been numerous reports on the use of gold nanoparticles as catalysts for olefin oxidation [2–7]. Haruta [8] reported the direct vapour-phase oxidation of propene with molecular oxygen in presence of hydrogen over Au/TiO₂ catalyst obtaining epoxide selectivity higher than 90% and propene conversion of 1–2% at 30–120 °C. Reaction rate was independent on the concentration of propene. It increased with increasing oxygen and hydrogen concentrations. Hayashi et al. [9] reported that propene

adsorbed on a gold surface reacts with *oxygen species* formed at the perimeter interface between Au particles and the TiO₂ support through the reaction of oxygen with hydrogen. Turner et al. [4] found that Au₅₅ nanocrystals supported on BN are catalytically active for styrene oxidation with dioxygen achieving nearly 20% conversion with an epoxide selectivity of 14%. They found a sharp size threshold in catalytic activity. The catalytic performance of Au was described as due to altered electronic structure intrinsic to particle size. Decreasing particle size is associated with an increase in the d-electron density of the gold atoms and the onset of reactivity with dioxygen. Zhu et al. [10] described the catalytic activity of thiolate-capped gold nanoclusters (Au₂₅(SR)₁₈) in neat and SiO₂ supported forms for selective oxidation of styrene with molecular oxygen. Benzaldehyde formed with 70% selectivity. Deng and Friend [2] presented selective oxidation of styrene on an oxygen-covered Au(111) surface and concluded that the oxidation depends on the ability of dissociating dioxygen, which can be tuned by support and quantum size effect. Yoke-shell nanospheres confined with ultra-small Au nanoparticles catalyzed styrene oxidation with oxygen at ambient pressure affording styrene oxide yield of over 30% at 100 °C in 15 h [11]. Many oxidation reactions proceed well with the most environmentally benign oxidant – molecular oxygen. However, in many other cases, such as epoxidation reactions, molecular oxygen does not work efficiently. In such cases, a far more reactive form of oxygen species (H_2O_2 or TBHP) is necessary to produce epoxides.

* Corresponding author at: Catalysis and Inorganic Chemistry Division, CSIR-National Chemical Laboratory, Pune 411 008, India.

E-mail address: d.srinivas@ncl.res.in (D. Srinivas).

Choudhary and co-workers [12–14] reported that Au supported on a range of oxides (MgO , CaO , SrO , BaO , Al_2O_3 , Ga_2O_3 , In_2O_3 , Ti_2O_3 , Cr_2O_3 , MnO_2 , Fe_2O_3 , CoO_x , NiO , CuO , ZnO , Y_2O_3 , ZrO_2 , La_2O_3 , Ce_2O_3 , Nd_2O_3 , Sm_2O_3 , Eu_2O_3 , Tb_2O_3 , Er_2O_3 , Yb_2O_3 and U_3O_8) is active for oxidation of styrene yielding styrene oxide (SO) with anhydrous TBHP (in benzene) as oxidant. Supports play a crucial role in catalytic reactions providing anchoring sites to metal nanoparticles and influencing the reaction rates. Yin et al. [15] studied the epoxidation of styrene over Au/mesoporous Al_2O_3 . Zhang et al. [16] elucidated the crystal face selective deposition of Au and the higher activity of Au nanoparticles of 2–3 nm deposited at lateral faces {10̄10} of a layered double hydroxide compound (LDH) in the oxidation of styrene by TBHP. Au_{25} clusters immobilized on hydroxyapatite (HAP) showed best catalytic performance for epoxidation of styrene in toluene medium [17]. Gold supported S- and ionic liquid fragments-containing periodic mesoporous organic silicas showed good oxidation activity with H_2O_2 as oxidant [18,19]. Development of easily scalable, efficient, epoxide selective and stable solid catalyst for styrene epoxidation is still a challenge. Further, the mechanism of oxidant activation and *reactive oxygen species* formed over Au during reactions are not fully understood.

Titanate nanotubes (TNT) are particularly attractive hosts for catalytically active metal nanoparticles because of their well-defined mesoporous one-dimensional structure, high specific surface area and ion-exchange capability [20–23]. Their semiconducting properties lead to strong support-metal interaction which could influence the catalytic performance of metal nanoparticles. We report here, for the first time, the catalytic activity of Au supported on barium titanate nanotubes (Au/BaTNT) in epoxidation of styrene with different oxidants such as O_2 , $\text{H}_2 + \text{O}_2$, aqueous H_2O_2 , aqueous TBHP and 5.5 M TBHP in decane. The influence of reaction parameters such as oxidant, solvent, Au loading (on BaTNT), catalyst amount, substrate/oxidant mole ratio, temperature and reaction time on the yield of styrene oxide is probed. The scope of Au(1 wt.%)/BaTNT for oxidation of a range of substituted styrenes is reported. Reusability of the catalyst is also probed. In situ UV-vis and FT-Raman spectroscopies are used to investigate the *reactive oxygen species* formed during the oxidation reaction. Earlier, we reported the use of gold supported on TNT for alcohol oxidation with molecular oxygen [24,25].

2. Experimental

Titanium dioxide (98%, anatase TiO_2), sodium hydroxide (NaOH) and barium nitrate were obtained from Thomas Baker Chemicals Ltd., Chloroauric acid ($\text{HAuCl}_4 \cdot 3\text{H}_2\text{O}$) was procured from HiMedia Chemicals Ltd. All reagents were used as received.

2.1. Catalyst preparation

BaTNT was prepared by ion-exchanging preformed sodium titanate nanotubes (NaTNT) with Ba^{2+} ions. In a typical preparation, 2.5 g of NaTNT (dried at 100 °C for 2 h) was added to 120 ml of aqueous $\text{Ba}(\text{NO}_3)_2$ solution (0.5 M) taken a beaker. The suspension was heated to 80 °C and stirred for 8 h. The solid was separated and the same procedure was repeated two more times. Then, the isolated solid was washed with deionized water and dried at 110 °C overnight to obtain BaTNT. The sodium form of titanate nanotubes (NaTNT) were prepared by alkali treatment of anatase titania [24–26].

In a typical preparation of Au/BaTNT, an appropriate amount of 2 mM aqueous solution of $\text{HAuCl}_4 \cdot 3\text{H}_2\text{O}$ was added drop-wise to 1 g of BaTNT suspended in 100 ml of deionized water followed by vigorous stirring at 80 °C for 12 h while keeping in dark. The solid formed was filtered, washed with deionized water and dried

at 110 °C for 20 h to obtain the final material. The materials were then reduced in flowing hydrogen at 250 °C for 2 h to yield the final catalysts with input Au loading of 0.5–5 wt.%.

2.2. Characterization techniques

Elemental composition ($\text{Au}^{0/+}$, Ba^{2+} and Na^+) of the catalysts was analyzed by Inductively Coupled Plasma-Optical Emission Spectroscopy (ICP-OES; Spectro Arcos). Powder X-ray diffraction (XRD) of the catalyst samples was done on a Philips X'Pert Pro diffractometer using $\text{Cu-K}\alpha_1$ radiation ($\lambda = 0.15406$ nm) and a proportional counter detector. Measurements were done in the scan range (2θ) of 5–80° at a scan speed of 4°/min. Textural properties of the catalysts [specific surface area (S_{BET}), pore volume (V_p) and average pore diameter (d_p)] were determined from N_2 physisorption studies conducted at –196 °C using a Quantachrome USA (Autosorb-1C) equipment. Prior to N_2 adsorption, the samples were evacuated at 200 °C for 2 h. It was calibrated using a reference alumina sample (supplied by Quantachrome, USA). The samples for transmission electron microscopy (TEM) analysis were prepared by drop casting the catalyst material (which is already dispersed in isopropanol) on a holey-carbon film supported by a 300 mesh copper TEM grid. The analysis was performed using a FEI Tecnai F20 instrument with a 200 kV field emission gun. The mean particle size of Au was determined by inspection of several micrographs taken from various positions. The mean particle diameter (d_{av}) was calculated using the formula: $d_{\text{av}} = 6 \sum n_i d_i^3 / \sum n_i d_i^2$, where n_i is the number of particles having a diameter of d_i . One hundred particles were chosen to determine the mean diameter of gold particles. A Shimadzu UV-2700 spectrophotometer equipped with an integrating sphere attachment (ISR 2200) was used to acquire diffuse reflectance UV-vis (DRUV-vis) spectra of the powder samples. BaSO_4 was used as a reference standard. The DRUV-vis spectra were recorded for bare BaTNT and Au/BaTNT and for the samples contacted with a known quantity of solvent (H_2O , acetonitrile–ACN), oxidant (H_2O_2 , TBHP) and/or styrene. FT-Raman spectra of the catalysts were recorded in the range 200–1500 cm^{-1} using a Horiba JY LabRaman HR 800 Micro Raman spectrometer with 630 nm exiting energy generated by a He-Ne laser operating at 20 mV. The strength and density of basic sites in the catalysts were determined by temperature-programmed desorption (TPD) studies on a Micromeritics Auto Chem 2910 instrument using CO_2 as probe molecule. In a typical experiment, 0.1 g of the catalyst was taken in a U-shaped quartz sample tube. The catalyst was pre-treated in He (30 ml/min) at 250 °C for 1 h, then it was cooled to 25 °C and a mixture of CO_2 in He (10 vol%) was fed to the sample (30 ml/min) for 1 h. Further, the sample was flushed with He (30 ml/min) for 1 h at 100 °C. Baseline was checked for stability before acquiring the data points in the temperature range of 100–500 °C. The area of the desorption peaks gave the amount of basic sites present in the catalysts. Acidity of the samples was estimated in a similar manner using NH_3 instead of CO_2 as probe molecule. X-ray photoelectron spectra (XPS) was recorded on a VG Microtech Multilab ESCA 3000 spectrometer with $\text{Al-K}\alpha$ radiation ($h\nu = 1486.6$ eV). The binding energy scale was referenced to the C 1s line at 284.6 eV.

2.3. Reaction procedure

Epoxidation of styrene over Au/BaTNT catalysts was carried out at atmospheric pressure taking 0.05 g of catalyst, 10 mmol of styrene, 10 mmol of anhydrous TBHP (5.5 M in decane) or 70% aqueous TBHP or 30% aqueous H_2O_2 in a glass reactor (25 ml) placed in an oil bath at 80 °C and fitted with a water-cooled reflux condenser and magnetic stirrer. The reaction was conducted for 15 h. After the completion of the reaction, the reactor was cooled to room temperature and then the catalyst was separated by cen-

trifugation. The reaction products and unconverted styrene were analyzed by gas chromatography (GC) [Varian 3400; column—CP-SIL 5 CB (30 m-long and 0.53 mm i.d. \times 0.25 μm)] and products were identified by GC-MS [Shimadzu GCMS-QP5050A; column-HP-5 (30 m-long \times 0.25 mm i.d. \times 0.25 μm thickness)] techniques. The effect of reaction conditions on catalyst performance was also studied. In a few experiments molecular oxygen or $\text{H}_2 + \text{O}_2$ was used as oxidant instead of peroxides.

3. Results and discussion

3.1. Catalyst characterization

3.1.1. Structural and textural properties

BaTNT showed characteristic XRD peaks at $2\theta = 10.1, 24.3, 28.4$ and 48.5° arising from (200), (110), (211) and (020) planes, respectively (JCPDS files: 31-1329 and 41-0192) (Supplementary data, S1). The XRD pattern of BaTNT was similar to that of NaTNT [25], confirming the isomorphous structure of these compounds. Thus the ion-exchange process had little effect on the titanate structure. Two additional peaks at $2\theta = 38.2$ and 44.6° originating from (111) and (200) planes of metallic Au (JCPDS files: 04-0784 and 05-068) appeared for Au/BaTNT compositions having input Au loadings of 3 and 5 wt.% (Supplementary data, S1). These additional peaks were absent for other Au/BaTNT samples (Au = 0.5, 1 and 2 wt.%) inferring that the crystallite size of Au in those catalyst samples was below the detection limit of X-rays. At higher gold loadings, some decrease in intensity and broadening of (200) peak [relative to (020)] was noted. This is due to blockage of inter planar spacing with Au nanoparticles or structural deformation as a consequence of strong interaction of Au with the support titanate nanotubes.

The chemical composition (Au, Ba^{2+} and Na^+ contents) of Au/BaTNT catalysts was determined by ICP-OES (Table 1). On loading Au, a significant decrease in Ba^{2+} content (from 17.76 to 9.26 wt.%) was noted. This decrease for Na^+ was marginal (from 0.43 to 0.40 wt.%) up to Au loading of 2 wt.% and above that the Na^+ content in the catalyst decreased to 0.28 wt.%. These observations point out that a part of Ba^{2+} and Na^+ was exchanged initially (prior to reduction with hydrogen) with Au ions in the deposition procedure. However, it may be noted that the decrease in the amount of Ba^{2+} was higher than expected (on the basis of Au deposited). It is likely that Cl^- ions in chloroauric acid (Au precursor used for deposition on BaTNT) must have reacted with Ba^{2+} ion and removed them as BaCl_2 from the solid titanate structure. The exchange positions must have been replaced with H^+ ions from chloroauric acid. Not all input Au got deposited on the TNT support. The actual value of Au present in the final composition was lower than the input value (Table 1).

Nitrogen adsorption-desorption isotherms (Supplementary data, S2) of “bare” and Au supported BaTNT showed type-IV behaviour with a H_2 -hysteresis loop and confirm the mesopore structure. With increasing Au loading, S_{BET} decreased gradually from 175 to 140 m^2/g , V_p decreased from 0.4 to 0.35 cc/g and d_p decreased from 6.0 to 5.1 nm (Table 1). These alterations in textural properties of BaTNT could be attributed to a change in chemical composition (loss of Ba^{2+} content and incorporation of Au metal particles and H^+ ions). This variation is in agreement with the observed changes (decrease in intensity and broadening of (200) peak) in the XRD pattern of Au/BaTNT catalysts. A careful examination of the pore size distribution plot (Supplementary data, S2) reveals the presence of two types of pores of 2 and 5 nm. While the larger pore corresponds to the inner diameter of the titanate nanotubes, the smaller pore corresponds intra-layer spacing within the walls of the multi-walled nanotubes.

TEM images revealed the presence of Au nanoparticles on the inner and outer surfaces of multi-walled hollow tubes of BaTNT (Fig. 1). The length of nanotubes ranged from several tens to hundreds of nanometers. The outer and inner diameters of BaTNTs were 10 and 5 nm, respectively. It is gratifying to note that the inner diameter value derived from TEM study is quite close to that obtained from N_2 -physisorption measurements (~ 5 –6 nm). The distribution of Au nanoparticles is uniform as could be seen from the TEM images of samples containing higher weight percentage of Au (2–5 wt.%; Fig. 1(c)–(e)). At lower loadings, ca., 0.5 wt.%, Au nanoparticles of size lower than 1 nm are also expected. But they could not be detected due to limitation on the TEM instrument we used. Only those NPs which are of size above 1 nm were clearly detected. These could be few in number at lower Au loadings. Thus, it appears, as if the Au nanoparticles are not uniformly distributed at lower loadings. However, this problem doesn't occur at higher Au loadings. In other words, from the visualization of TEM images it can be concluded that the Au nanoparticles are relatively well distributed and decorated on the walls of nanotubes. The mean particle size (d_{av}) and percentage dispersion of Au estimated from TEM images are listed in Table 1. As the gold loading increased from 0.5 to 5 wt.%, d_{av} of Au increased from 5.0 to 7.4 nm with a concomitant decrease in Au dispersion from 22 to 15%. An inverse relation was observed also between Au particle size and the textural properties (S_{BET} & d_p ; Fig. 2). These observations reveal that deposition of Au induces structural changes in BaTNT.

Acidic and basic properties of the catalysts and the influence of Au loading on these properties were investigated by TPD measurements. CO_2 -TPD profiles (Supplementary data, S3) showed two overlapping desorption peaks in the temperature regions 100–300 and 300–500 °C corresponding to weak and strong basic sites, respectively. As the Au loading increased, the amount of strong basic sites decreased while the weak basic sites increased. The T_{max} of desorption peaks shifted to higher temperatures with increase in Au loading. As the metal loading increased, the overall basic site density of the catalyst sample decreased from 3.65 to 2.06 $\mu\text{mol}/\text{m}^2$ (Table 1). NH_3 -TPD of BaTNT (Supplementary data, S4) showed two broad overlapping peaks with maximum at 200 and 295 °C attributable to weak and strong Lewis acid sites, respectively. Deposition of Au created Brönsted acid sites on BaTNT surface which exhibited a characteristic NH_3 -TPD band at 376 °C. Intensity of this new band increased with increasing Au loading. The overall acidity of BaTNT increased from 0.89 to 2.46 $\mu\text{mol}/\text{m}^2$ as the loading of Au increased from 0 to 5 wt.% (Table 1). Elemental analysis (Table 1) pointed out depletion of Ba^{2+} and Na^+ ion contents on Au deposition. The extent of Ba^{2+} depletion was more than the amount of Au that got deposited. This concludes that a portion of alkali ions ($\text{Ba}^{2+}/\text{Na}^+$) was exchanged with H^+ ions from chloroauric acid and as a consequence of that new Brönsted acid centres were created in Au-loaded BaTNT samples. These centres showed a NH_3 -TPD peak at 376 °C. With increasing Au loading, Ba^{2+} ion content and the density of basic sites had decreased while the Brönsted acid sites on TNT had increased (Supplementary data, S5).

3.1.2. Spectral properties

The chemical environment of supported Au catalysts was probed by XPS. Metallic gold shows $4f_{7/2}$ line in XPS at 84.0 eV [27]. For Au(1 wt.%)/BaTNT, this spectral line appeared at a lower binding energy (B.E.) value of 82.8 eV (Supplementary data, S6) due to support-metal interactions. The shift of $\text{Au}4f_{7/2}$ to lower B.E. value suggests that the surface of Au nanoparticles in Au/BaTNT catalysts is richer in electron density. This increase in electron density at Au is due to a consequence of transfer of electron density from the support BaTNT to metal particles [25]. Another set of low intensity signals at higher B.E. values assignable to $\text{Au}^{\delta+}$ ions was also observed. The ratio of $\text{Au}^{\delta+}/\text{Au}^0$ species in Au(1 wt.%)/BaTNT was

Table 1

Physicochemical properties of Au/BaTNT catalysts.

Catalyst	Elemental analysis (wt%) ^a			Textural properties ^b			Average particle size of Au (d _{av} , nm) ^c	Dispersion of Au (%) ^c	Basicity (μmol/m ²) ^d			Acidity (μmol/m ²) ^e		
	Au	Ba	Na	S _{BET} (m ² /g)	V _p (cc/g)	d _p (nm)			Weak	Strong	Total	Weak	Strong	Total
BaTNT	—	17.76	0.43	175	0.40	6.0	—	—	0.28	3.37	3.65	0.35	0.54	0.89
Au(0.5 wt.%)/BaTNT	0.30	15.64	0.42	162	0.39	5.6	5.0	22	0.30	2.94	3.24	0.42	0.63	1.05
Au(1 wt.%)/BaTNT	0.68	13.81	0.42	155	0.37	5.4	5.2	20	0.21	2.79	3.0	0.43	0.84	1.27
Au(2 wt.%)/BaTNT	1.46	12.97	0.40	150	0.36	5.4	5.9	19	0.27	2.36	2.63	0.33	1.50	1.83
Au(3 wt.%)/BaTNT	2.80	12.00	0.36	146	0.36	5.3	7.0	16	0.32	2.07	2.39	0.48	1.56	2.04
Au(5 wt.%)/BaTNT	4.10	9.26	0.28	140	0.35	5.1	7.4	15	0.42	1.72	2.06	0.55	1.91	2.46

^a ICP-OES.^b N₂-physisorption.^c TEM.^d CO₂-TPD.^e NH₃-TPD.

determined to be 0.43. It is likely that a portion of Au is present in ion exchange form (Au^{δ+}). Titanates are well known for their ion exchange ability. The ion exchange Au represents a higher binding energy position in our X-ray photoelectron spectrum. This finding is in agreement with that reported by Pusztai et al. [28].

DRUV-vis spectroscopy is a sensitive technique to probe the local environment of Au nanoparticles. The characteristic localized surface plasmon resonance (LSPR) band of Au/BaTNT was observed at 545–580 nm (Fig. 3(i)). The position and shape of this plasmonic band is dependent on the size of metallic nanoparticles. Shift in the LSPR band from the near-UV through the visible region and even into the near IR region is related to change in the size and shape of the nanoparticles. With increasing Au loading, a red shift in LSPR band position (λ_{max}) and increase in intensity of the band were observed (Fig. 3(i)). Increase in the particle size of Au and decrease in metal dispersion (Table 1) are the causes for this observation [29].

FT-Raman spectroscopy of anatase TiO₂ showed four main peaks at 141, 396, 517 and 641 cm⁻¹ corresponding to E_g, B_{1g}, A_{1g} and E_g mode vibrations, respectively. BaTNT and Au/BaTNT (Fig. 3(ii)) showed characteristic peaks at 275–290, 433–450 and 706 cm⁻¹ corresponding to titanate nanotube structure [30]. FT-Raman spectrum confirmed the purity of titanate samples by showing the absence of anatase TiO₂ peaks. The mode at 275–290 cm⁻¹ is assigned to vibrations involving Ti–O–Ba²⁺ groups. The bands at 433–450 and 706 cm⁻¹ are assigned to Ti–O bending vibrations in TiO₆ octahedron [31]. The band at 890 cm⁻¹ corresponding to the short Ti–O bond vibration in TiO₆ octahedron of titanate nanotubes disappeared after deposition of gold. The band at 275–290 cm⁻¹ (which was assigned to long Ti–O bond) shifted to higher frequency (lower wave number). The short and long Ti–O bonds are the bonds between central Ti atom and terminal oxygen atoms and the bonds between Ti and bridge oxygen atoms in the octahedron, respectively. A new band at 150 cm⁻¹ observed for Au/BaTNT indicates the slight deformation of titanate structure on Au deposition. Similar observations were reported also by Yang et al. [32].

3.2. Catalytic activity

Catalytic epoxidation of styrene was investigated with O₂, H₂ and O₂ mixture, 30% aq. H₂O₂, 70% aq. TBHP and TBHP in decane (5.5 M) as oxidants. The oxidation of styrene with molecular oxygen was ineffective in the absence of catalyst at our reaction conditions (styrene = 10 mmol, solvent = acetonitrile (ACN, 5 ml), temperature = 80 °C, reaction time = 15 h) (Table 2). But it occurred to a less extent even in the absence of a catalyst when peroxides instead of molecular oxygen were employed as oxidant [styrene conversion = 10.1% (with aq. H₂O₂), 13.4% (with aq. TBHP), 18.0 wt.%

(with TBHP in decane); Table 2]. Styrene oxide (SO), benzaldehyde (Bzh), phenylacetaldehyde (PAA), 1-phenyl-1,2-ethanediol (Diol) and others including acids (phenylacetic acid and benzoic acid) were the products of styrene oxidation (Scheme 1). While Bzh was the major product (selectivity = 61.2 wt.%) in the oxidation with aq. H₂O₂ (Table 2, Run No. 2), SO (32.3 and 38.9 wt.%) and others (35.7 and 27.5 wt.%) formed in higher amounts than Bzh (25.8 and 26.1 wt.%) in reactions with TBHP (Table 2, Run Nos. 3 and 4). In the presence of “bare” BaTNT (and TBHP in decane oxidant), styrene conversion increased from 18.0 to 22.5 wt.% with SO and Bzh forming in near equal amounts (43.0 and 41.2 wt.%, Table 2, Run No. 5). Basicity of the support enhanced the oxidation rate to SO and Bzh while limiting the formation of over oxidized products (from 27.5 to 9.8 wt.%). Oxidation of styrene enhanced still further when the reaction was conducted in presence of supported Au catalysts (compare Run Nos. 6–16 with 1–5). With molecular oxygen as oxidant, the conversion of styrene over Au(1 wt.%)/BaTNT was 1.0 wt.% with Bzh forming in 100% selectivity. When an equal volume mixture of H₂ and O₂ was employed, conversion of styrene increased from 1.0 to 19.3 wt.% over the supported Au catalyst (compare Run No. 7 with 6). Gold catalysts are known to produce hydrogen peroxide *in situ* from H₂ + O₂ mixtures [33,34]. In situ formed H₂O₂ functioned as an oxidant in this reaction. When the oxidation was carried out with 30% aq. H₂O₂, conversion of styrene increased to 34.4 wt.% (Run No. 8). Some difference in product selectivity was noted in Run Nos. 7 and 8 (using H₂ + O₂ and aq. H₂O₂). This difference is due to difference in the amount of H₂O₂ available for the reaction at the active sites and the water content (while the former contains no water in the medium, aq. H₂O₂ in the latter has 70% water). This study, thus, reveals that Au/BaTNT catalysts are efficient for *in situ* production of H₂O₂ from H₂ and O₂ for oxidations. In fact, Torrente-Murciano et al. [35,36] did observe enhanced hydrogen peroxide productivity (above 11 600 mol/kgmetal/h) over Au-Pd alloy supported on titanate nanotubes due to high metal-support interaction in those materials. In a tandem-type reaction, the in situ formed hydrogen peroxide was utilized in the selective oxidation of salicylic acid to aldehyde. This in situ utilization minimized the parallel decomposition of hydrogen peroxide overcoming one of the limitations on the use of H₂O₂ as a green oxidant [36].

Styrene conversion and SO selectivity/yield enhanced when TBHP instead of H₂O₂ was used as oxidant (Table 2, Run Nos. 9–16). With aq. TBHP (70%), styrene conversion was 46.8 wt.% and SO selectivity and yield were 70.9 and 33.2 wt.%, respectively. While using TBHP in decane (5.5 M) as oxidant, styrene conversion over Au(1 wt.%)/BaTNT reached 60.5 wt.% and SO selectivity and yield to 80.1 and 48.5 wt.%, respectively. Conversion of styrene increased (from 31.0 to 80.0 wt.%) with increasing Au loading (from 0.5 to 5 wt.%) on BaTNT (compare Run Nos. 10–14). However, the

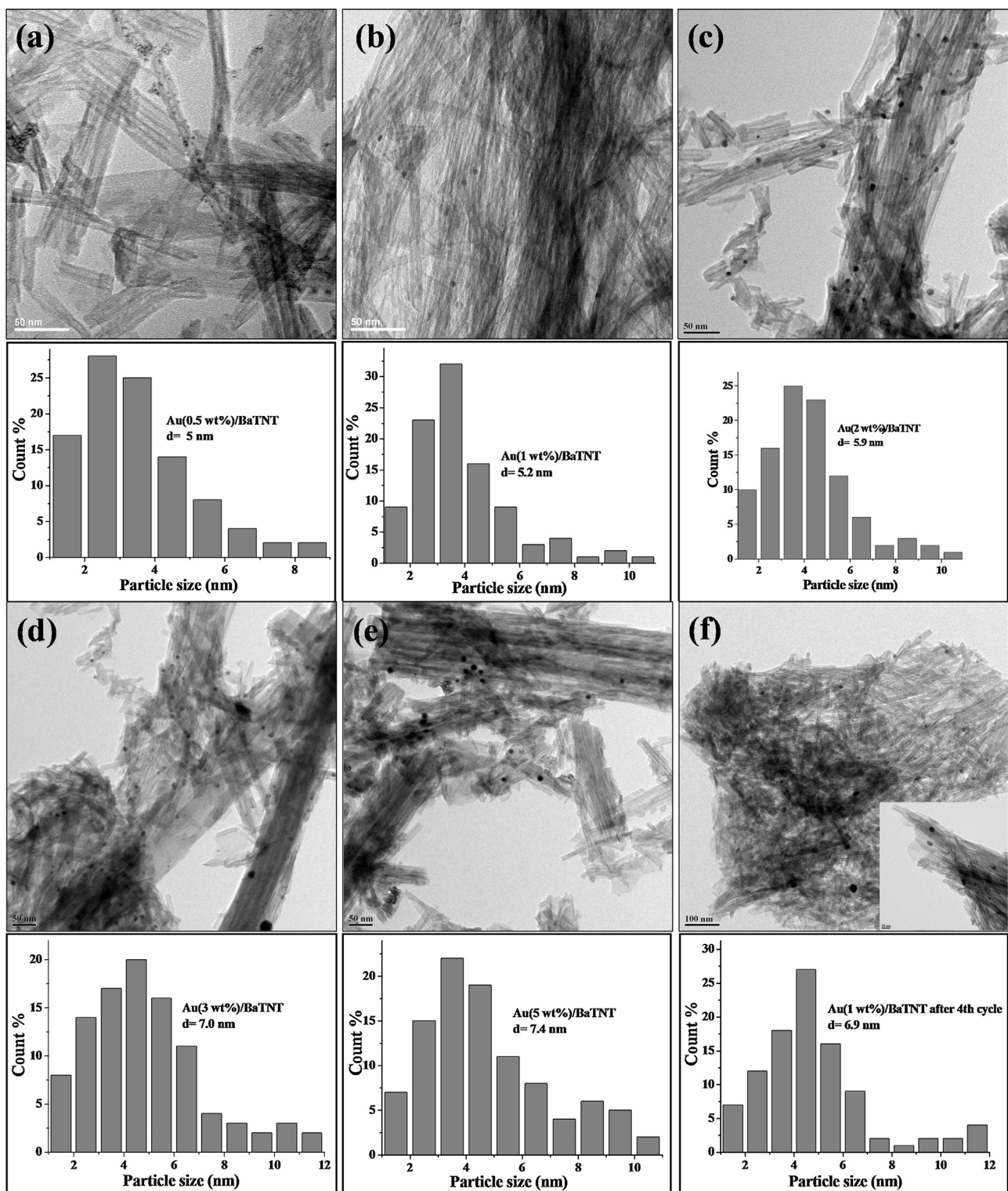


Fig. 1. TEM images and particle size distribution curves of (a) Au(0.5 wt%)/BaTNT (b) Au(1 wt%)/BaTNT (c) Au(2 wt%)/BaTNT (d) Au(3 wt%)/BaTNT (e) Au(5 wt%)/BaTNT and (f) Au(1 wt%)/BaTNT after use in 4th cycle.

increase in conversion was less significant at higher Au loadings. SO selectivity increased up to Au loading of 1 wt.% and above that it decreased. TEM studies (Fig. 1, Table 1) revealed that the mean particle size of Au increases from 5 to 7.4 nm as the gold loading increases above 1 wt.%. Perhaps this increment in Au diameter hampers the catalytic activity (TOF). Fast decomposition of TBHP may also be a reason with increase in gold loading leading to

decrease in catalytic activity. On the other hand, the selectivity of SO increases to as high as 80.1 wt.% (from 75.8 wt.%) as the Au loading increases from 0.5 to 1 wt.% and further increase in Au loading causes decrease in SO selectivity. A marginal increase in PAA (from 3.4 to 12.5 wt.%) and Bzh (14.0–16.1 wt.%) selectivity was noted with increase in Au loading. Thus, these studies point out that Au loading and oxidant type have significant effects on

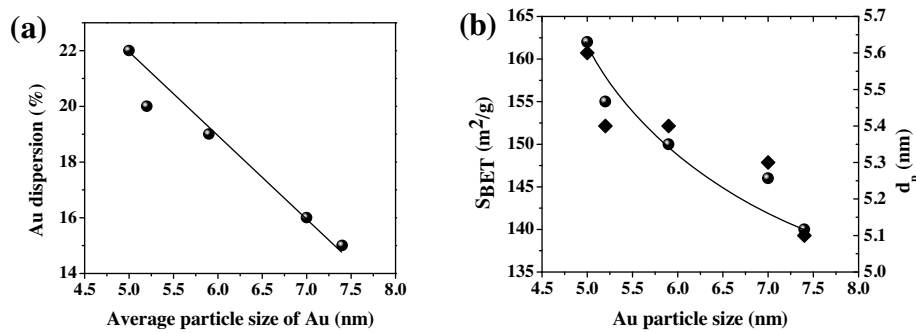


Fig. 2. Correlation between average Au particle size (from TEM) and (a) Au dispersion and (b) S_{BET} (●) and d_p (◆).

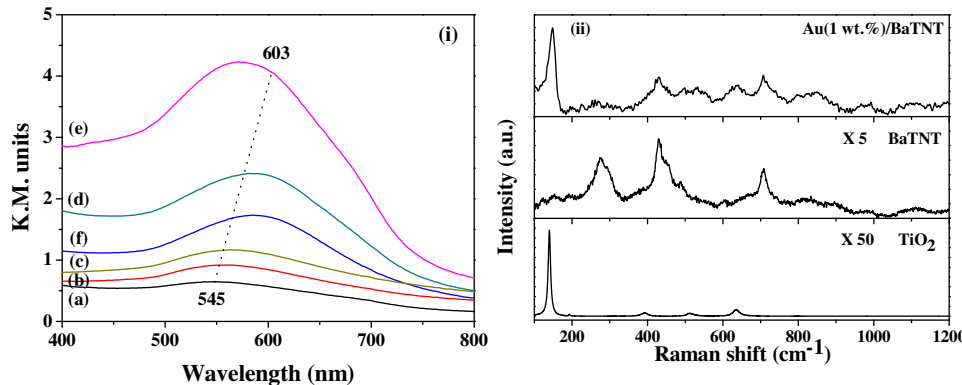


Fig. 3. (i) DRUV-vis spectra of (a) Au(0.5 wt.%)/BaTNT (b) Au(1 wt.%)/BaTNT (c) Au(2 wt.%)/BaTNT (d) Au(3 wt.%)/BaTNT, (e) Au(5 wt.%)/BaTNT and (f) Au(1 wt.%)/BaTNT after use in 4th cycle. (ii) FT-Raman spectra of TiO₂, BaTNT and Au(1 wt.%)/BaTNT. The FT-Raman spectra of BaTNT after five times intensity magnification (×5) and TiO₂ after 50 times intensity magnification (×50) are shown.

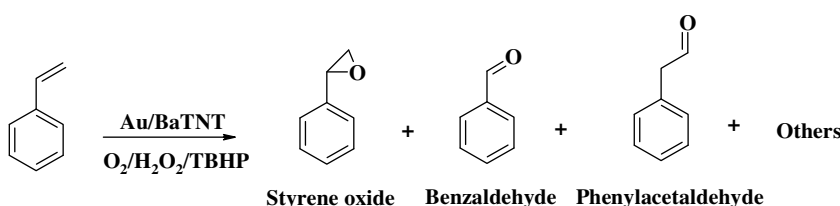
Table 2

Catalytic activity data of Au/BaTNT in epoxidation of styrene^a.

Run No.	Catalyst	Oxidant	Styrene conversion (wt.%)	Product selectivity (wt%)					Yield of SO (%)	TOF ^b (h ⁻¹)
				SO	Bzh	PAA	Diol	Others		
1	–	O ₂ (10 ml/min)	0.0	–	–	–	–	–	–	–
2	–	Aq. H ₂ O ₂ (30%)	10.1	17.1	61.2	5.5	12.7	3.5	1.7	–
3	–	Aq. TBHP (70%)	13.4	32.3	25.8	6.2	0	35.7	4.3	–
4	–	TBHP in decane (5.5 M)	18.0	38.9	26.1	7.5	0	27.5	7.0	–
5	BaTNT	TBHP in decane (5.5 M)	22.5	43.0	41.2	6.0	0	9.8	15.1	–
6	Au(1 wt.%)/BaTNT	O ₂ (10 ml/min)	1.0	–	100	–	–	–	–	4.9 (13)
7	Au(1 wt.%)/BaTNT	H ₂ + O ₂ (10 ml/min each)	19.3	35.8	53.6	0	0	10.6	6.9	75 (251)
8	Au(1 wt.%)/BaTNT	Aq. H ₂ O ₂ (30%)	34.4	22.8	54.0	1.7	19.3	2.2	7.8	134 (447)
9	Au(1 wt.%)/BaTNT	Aq. TBHP (70%)	46.8	70.9	18.9	4.8	0	5.4	33.2	182 (608)
10	Au(0.5 wt.%)/BaTNT	TBHP in decane (5.5 M)	31.0	75.8	14.0	3.4	0	6.8	23.5	273 (879)
11	Au(1 wt.%)/BaTNT	TBHP in decane (5.5 M)	60.5	80.1	13.4	2.5	0	4.0	48.5	236 (786)
12	Au(2 wt.%)/BaTNT	TBHP in decane (5.5 M)	72.8	74.2	13.8	5.6	0	6.4	54.0	132 (500)
13	Au(3 wt.%)/BaTNT	TBHP in decane (5.5 M)	77.2	69.4	14.1	9.9	0	6.6	53.6	73 (328)
14	Au(5 wt.%)/BaTNT	TBHP in decane (5.5 M)	80.0	64.6	16.1	12.5	0	6.8	51.7	52 (246)
15	Au(1 wt.%)/BaTNT	TBHP in decane (5.5 M) + O ₂ (static)	72.2	34.0	59.9	2.3	0	3.8	24.5	281 (938)
16	Au(1 wt.%)/BaTNT	TBHP in decane (5.5 M) + O ₂ (10 ml/min)	75.8	56.1	34.8	1.4	0	7.7	42.5	295 (985)

^a Reaction conditions: catalyst = 50 mg, styrene = 10 mmol, solvent (acetonitrile) = 5 ml, reaction temperature = 80 °C, substrate/oxidant (H₂O₂/TBHP) ratio (mol/mol) = 1, reaction time = 15 h. SO = styrene oxide, Bzh = benzaldehyde, PAA = phenylacetaldehyde, Diol = 1-phenyl-1, 2-ethanediol and others include acids.

^b Turnover frequency (TOF) = moles of styrene converted per mole of total Au in the catalyst (ICP-OES) per hour. Values in parentheses were calculated based on the formula: moles of styrene converted per mole of surface Au atoms (TEM) per hour.



Scheme 1. Products in the oxidation of styrene over Au/BaTNT catalysts.

Table 3Effect of solvent on the catalytic performance of Au(1 wt.%)/BaTNT^a.

Run No.	Solvent	Styrene conversion (wt.%)	Product selectivity (wt.%)				Yield of SO (%)
			SO	Bzh	PAA	Others	
1	Acetonitrile	60.5	80.1	13.4	2.5	4.0	48.5
2	N,N-dimethylformamide	38.8	70.0	23.0	0	7.0	27.2
3	N,N-dimethylacetamide	20.7	45.0	45.4	0	9.6	9.3
4	1,4-Dioxane	14.6	57.4	36.1	0	6.5	8.4
5	Toluene	15.4	39.6	48.8	4.4	7.2	6.1

^a Reaction conditions: catalyst = 50 mg, styrene = 10 mmol, solvent = 5 ml, reaction temperature = 80 °C, substrate/TBHP (5.5 M in decane) (mol/mol) = 1:1, reaction time = 15 h. SO = styrene oxide, Bzh = benzaldehyde, PAA = phenylacetaldehyde, Diol = 1-phenyl-1,2-ethanediol and others include acids.

Table 4Influence of reaction temperature on the epoxidation of styrene over Au(1 wt.%)/BaTNT^a.

Run No.	Temp. (°C)	Styrene conversion (wt.%)	Product selectivity (wt.%)				Yield of SO (%)	TOF ^b (h ⁻¹)
			SO	Bzh	PAA	Others		
1	40	20.0	58.4	18.2	1.2	22.2	11.7	78 (260)
2	60	31.4	69.4	16.8	3.0	10.8	21.8	122 (408)
3	80	60.5	80.1	13.4	2.5	4.0	48.5	236 (786)
4	85	64.4	73.6	13.8	2.8	9.8	47.4	251 (837)

^a Reaction conditions: catalyst = 50 mg, styrene = 10 mmol, solvent (acetonitrile) = 5 ml, substrate/TBHP (5.5 M in decane) (mol/mol) = 1:1, reaction time = 15 h.

^b Turnover frequency (TOF) = moles of styrene converted per mole of total Au in the catalyst (ICP-OES) per hour. Values in parentheses were calculated based on the formula: moles of styrene converted per mole of surface Au atoms (TEM) per hour.

the epoxidation reaction. Teranishi et al. [34] found an unique activity- d_{av} relation in the Au/TiO₂-photocatalyzed H₂O₂ formation. Both formation and decomposition of H₂O₂ mainly occur at the reduction sites on the Au surface (i.e., Au-TiO₂ interfaces and/or low-coordinated Au atoms). The Au surface area of Au/TiO₂ decreases inversely with d_{av} . This, in turn, effects the active sites and H₂O₂ production. Similar causes are responsible even in the present case, for the observed variations in conversion and SO selectivity with increased Au loading. TBHP in decane enabled higher yields of SO and higher turnover frequency (TOF = moles of styrene converted per mol of total or surface Au per hour). When molecular oxygen was co-dosed with TBHP in decane, styrene conversion increased still further (from 60.5 to 75.8 wt.%), but the selectivity of SO decreased (compare Run Nos. 11, 15 and 16). TOF values for styrene oxidation over Au/BaTNT catalyst increased with different oxidants in the order: O₂ < H₂ + O₂ < aq. H₂O₂ < aq. TBHP < TBHP(in decane) < TBHP + O₂. With TBHP + O₂ oxidant, TBHP (through t-BuO[•]/HO[•]) initiates the activation of dioxygen forming *active oxygen species* (O₂[−]) which may be responsible for the enhanced conversion and low SO selectivity [37]. It is known that hydroperoxo/peroxy species are responsible for selective epoxidation while superoxo species (O₂[−]) lead to non-selective products [38]. Enhanced conversion and selectivity to SO were obtained in the case of O₂ flow compared to the static condition. Such observations were reported also by others [39].

Solvent has a remarkable effect on the epoxidation of styrene at 80 °C over Au(1 wt.%)/BaTNT using TBHP (5.5 M, in decane) as oxidant (Table 3). At the chosen conditions, highest catalytic activity (60.5 wt.%) and SO selectivity (80.1 wt.%) were obtained in acetonitrile solvent medium. Conversion of styrene in different solvents decreased in the order: 1,4-dioxane < toluene < N,N-dimethylacetamide < N,N-dimethylformamide < acetonitrile. While SO selectivity was higher in acetonitrile (80.1 wt.%) and N,N-dimethylformamide (70.0 wt.%), it was lower in toluene (39.6 wt.%), N,N-dimethylacetamide (45.0 wt.%) and 1,4-dioxane (57.4 wt.%). In general, polar solvents led to higher conversion and epoxide selectivity. Similar observations were made also by Liu et al. [40].

Au/BaTNT catalysts were active even at 40 °C for the epoxidation of styrene with TBHP in decane. Styrene conversion increased (from 20.2 to 64.4 wt.%) with increasing reaction temperature (from

40 to 85 °C). Also the selectivity for SO increased with temperature up to 80 °C and decreased thereafter. Therefore, 80 °C was considered as optimum reaction temperature for styrene oxidation to SO (Table 4).

Fig. 4(i) demonstrates the effect of catalyst amount on the catalytic performance of Au(1 wt.%)/BaTNT. Conversion of styrene increased from 24.6 to 82.4 wt.% with increase in catalyst/styrene mass ratio from 0.024 to 0.096, which could be attributed to the availability of more number of active sites. The SO selectivity was maximum at 80.1 wt.% when the catalyst/styrene mass ratio was 0.048. It decreased with increasing amount of catalyst due to further oxidation caused by the availability of more number of active sites. Thus, there was an upper limit of 0.048 for catalyst/styrene mass ratio for the chosen reaction conditions to get appreciable conversion and SO selectivity. Styrene conversion increased with increasing amount of oxidant (TBHP in decane) concentration (Fig. 4(ii)). SO selectivity increased marginally with substrate to TBHP molar ratio of 1:1 and above that it decreased. Thus, we arrived at a conclusion that a substrate to TBHP molar ratio of 1:1 was optimum to get higher SO yield. The course of the reaction was followed for 24 h at 80 °C and with a substrate to TBHP molar ratio of 1:1 (Fig. 4(iii)). Conversion of styrene increased with increasing reaction time, reaching a value of 78.8 wt.% at 24 h. Selectivity for SO also increased till 15 h of reaction and above that the change was not appreciable. Benzaldehyde and other products selectivity decreased with time till 15 h. All these observations reveal that reaction time of 15 h is ideal for high conversion and SO yield. The change in selectivity with time suggests a possible change in Au structure with time up to 15 h and above that the structure stabilizes [Fig. 4(iii)].

In order to establish the generality of Au(1 wt.%)/BaTNT catalyst for epoxidation reactions, a variety of substituted styrenes were tested under optimized reaction conditions (Table 5). α-Methylstyrene, p-methylstyrene and α,p-dimethylstyrene were converted with efficiencies comparable or more than that of styrene. Higher amount of epoxide yield was obtained for α,p-dimethylstyrene due to electron induced substitution effects. Electron withdrawing p-chloro and p-nitro substituents led to lower conversions and SO selectivity. p-Methoxy substitution has an adverse effect on the reaction. Electronegative substituents facilitated aldehyde selectivity. In other words, substituents (Table 5),

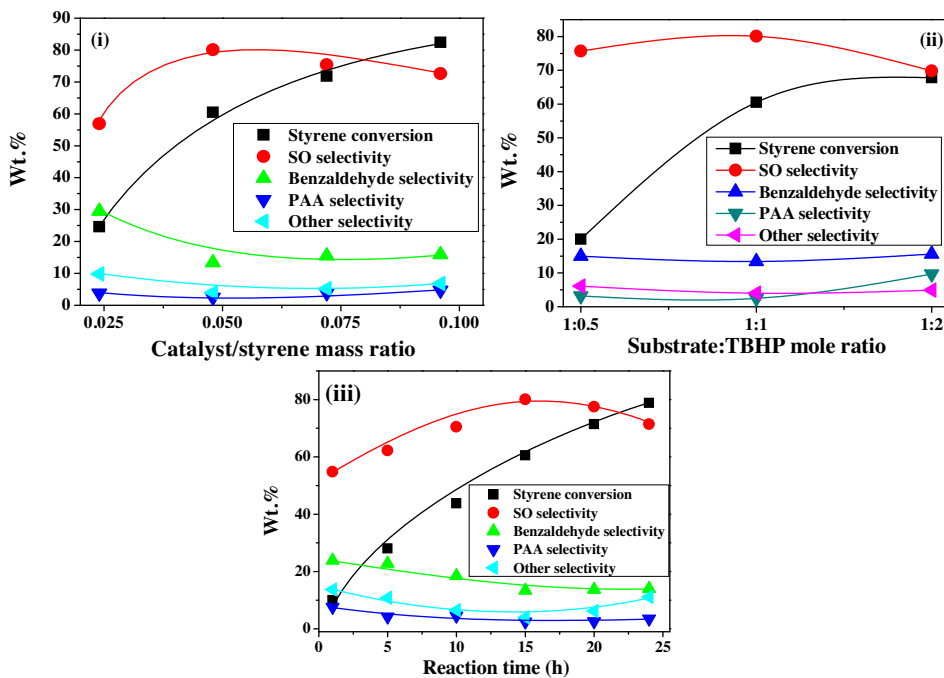


Fig. 4. Effect of reaction parameters—(i) catalyst amount (ii) substrate/TBHP (5.5 M in decane) molar ratio and (iii) reaction time on epoxidation of styrene over Au(1 wt. %)/BaTNT catalyst. Reaction conditions—for (i): styrene = 10 mmol, solvent (ACN) = 5 ml, reaction temperature = 80 °C, substrate/TBHP (mol/mol) = 1:1, reaction time = 15 h; for (ii): catalyst = 50 mg, styrene = 10 mmol, solvent (ACN) = 5 ml, reaction temperature = 80 °C, reaction time = 15 h; for (iii): catalyst = 50 mg, styrene = 10 mmol, solvent (ACN) = 5 ml, reaction temperature = 80 °C, substrate/TBHP (mol/mol) = 1:1.

Table 5
Epoxidation of substituted styrenes with TBHP over Au(1 wt. %)/BaTNT^a.

Run No.	Substrate	Conversion (wt.%)	Selectivity (wt.%)				Yield of epoxide (%)
			Epoxide	Bzh	PAA	Others	
1	Styrene	60.5	80.1	13.4	2.5	4.0	48.5
2	α-Methylstyrene	64.8	82.6	9.5	2.0	5.8	53.5
3	p-Methylstyrene	61.6	77.4	11.2	4.5	6.9	47.7
4	o,p-Dimethylstyrene	68.5	85.5	8.6	3.4	2.5	58.6
5	p-Chlorostyrene	48.8	61.2	28.0	4.4	6.4	29.9
6	p-Nitrostyrene	38.1	54.3	35.1	4.1	6.5	20.7
7	p-Methoxystyrene	32.8	68.3	15.9	6.3	9.5	22.4

^a Reaction conditions: catalyst = 50 mg, substrate = 10 mmol, solvent (acetonitrile) = 5 ml, reaction temperature = 80 °C, substrate/TBHP (5.5 M; in decane) (mol/mol) = 1:1, reaction time = 15.

nature of oxidant and Au loading (or particle size of Au; Table 2) showed an influence on styrene conversion and epoxide selectivity.

Epoxidation of styrene was followed as a function of time at four different temperatures (40, 50, 80 and 85 °C) over Au(1 wt. %)/BaTNT catalyst (Supplementary data, S7). The initial rates of reaction at different temperatures were calculated from the conversion versus time plots. Then the rate constant (k) was determined considering a pseudo-first order rate law. Activation energy value (E_a) estimated from the Arrhenius plot was found to be 16.7 kJ/mol.

3.2.1. Catalyst recyclability and spent catalyst characterization

With a view to examine the stability of the catalyst (Au(1 wt. %)/BaTNT) during reactions, recycle tests were conducted and the results for four subsequent recycles are shown in Fig. 5. After each run, the catalyst was separated from the reaction mixture by filtration, washed with acetonitrile, dried at 110 °C for 4 h and then, reused in the next recycle conducted at the same reaction conditions. A marginal decrease in styrene conversion from 60.5 wt.% (in the first run) to 55.4 wt.% (after the 4th recycle) was observed. The selectivity for SO was almost the same in all the recycle experiments. This loss in activity (~5 wt.%) could be attributed to losses in catalyst recovery at the end of each recycle.

Chemical and structural stability of the spent catalyst (at the end of 4th recycle) was investigated. While the ICP-OES analysis of spent catalyst revealed no loss in Au content, TEM study pointed out an increase in the average particle size of Au from 5.2 to 6.9 nm (Fig. 1(f)). The characteristic XRD peak corresponding to Au crystallites was more apparent in the case of spent catalyst than for the fresh catalyst (Supplementary data, S1) revealing increased crystallite size of Au in the spent catalyst. Further, an obvious red shift in LSPR band position of Au from 557 to 588 nm was observed for the spent Au(1 wt. %)/BaTNT catalyst (Fig. 3(i), traces (b) and (f)). This shift in DRUV-vis band position is accounted for an increase in the particle size of Au nanoparticles on BaTNT after their reuse in oxidation reactions. Thus, in addition to losses in catalyst recovery at the end of each recycle, the relative increase in the particle of Au nanoparticles (from 5.2 to 6.9 nm) also contributes to the marginal loss in styrene conversion (by 5 wt.%) observed in catalyst recycle experiments. Table 6 compares the catalytic activity data of different supported Au catalysts. Au(0.5 wt. %)/HAP resulted in 100% conversion and 92% SO selectivity. However, in that reaction, the oxidant ratio was much higher than that used in the present study. Au(1 wt. %)/CeO₂-rods enabled 99% conversion but SO selectivity was 44% only. Au(0.3 wt. %)/CNT showed high TOF (273 h⁻¹). The

Table 6

Catalytic activity of supported gold catalysts for styrene epoxidation.

Catalyst	Reaction conditions: amounts of styrene, catalyst, solvent and TBHP, and reaction temperature and reaction time	Styrene conversion (%)	Epoxide selectivity (%)	TOF (h^{-1})	Refs.
Au(6.6 wt.%)/Yb ₂ O ₃	10 mmol, 100 mg, 15 mmol (26% TBHP in benzene), 80 °C, 3 h	63.5	54.8	34.5	[5]
Au(4.1 wt.%)/MgO	10 mmol, 100 mg, 15 mmol (26% TBHP in benzene), 80 °C, 3 h	44.6	36.1	73.0	[14]
Au(7.5 wt.%)/MgO	10 mmol, 100 mg, 15 mmol (26% TBHP in benzene), 80 °C, 3 h	62.6	54.3	29.8	[14]
Au(4.7 wt.%)/CaO	10 mmol, 100 mg, 15 mmol (26% TBHP in benzene), 80 °C, 3 h	53.6	60.2	86.5	[14]
Au(5.3 wt.%)/BaO	10 mmol, 100 mg, 15 mmol (26% TBHP in benzene), 80 °C, 3 h	55.9	53.5	73.0	[14]
Au(0.3 wt.%)/CNT	4 mmol, 50 mg, 5 ml (acetonitrile), 3 ml (TBHP), 80 °C, 10 h	67.2	77.5	273	[41]
Au(0.05 wt.%)/HAP	0.38 mmol, 50 mg, 10 ml (toluene), 200 mg (TBHP), 80 °C, 12 h	100	92.0	114.0	[17]
Au(0.66 wt.%)/LDH	10.18 mmol, 100 mg, 5 ml (benzene), 28.58 mmol (TBHP), 80 °C, 8 h	67.4	73.5	157.2 ^a	[16]
Au(6.4 wt.%)/Al ₂ O ₃	10 mmol, 100 mg, 15 mmol (26% TBHP in benzene), 80 °C, 3 h	44.0	28.0	11.4	[42]
Au(4.0 wt.%)/silica	8 mmol, 200 mg, 4.5 ml (acetonitrile), 0.5 ml (DMF), 2 ml (70% TBHP in water), 80 °C, 14 h	42.1	83.9	99.4	[43]
Au ₂₅ (1 wt.%)–CeO ₂ rods	12 mmol, 100 mg, 15 ml (acetonitrile), 36 mmol (TBHP), 80 °C, 24 h	99	44	97.0	[44]
Au(1 wt.%)/meso-Al ₂ O ₃	10 mmol, 100 mg, 5 ml (benzene), 15.4 mmol (TBHP in decane, 5.5 M), 82–83 °C, 12 h	68.5	74.7	112	[15]
Au(1 wt.%)/BaTNT	10 mmol, 50 mg, 5 ml (acetonitrile), 10 mmol (TBHP in decane, 5.5 M), 80 °C, 15 h	60.5	80.1	236 (786 ^a)	This work

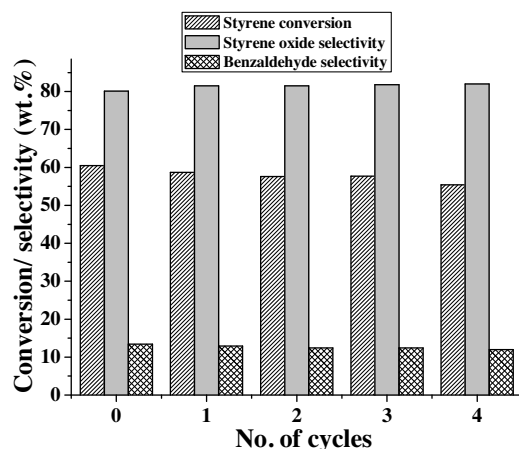
^a TOF obtained using moles of surface Au atoms.

Fig. 5. Catalyst recyclability study. Reaction conditions: catalyst—Au(1 wt.%)/BaTNT = 50 mg, styrene = 10 mmol, solvent (ACN) = 5 ml, reaction temperature = 80 °C, substrate/TBHP (5.5 M in decane) (mol/mol) = 1:1, reaction time = 15 h.

catalyst of the present study showed comparable or higher catalytic performance (TOF and SO selectivity) than the reported catalysts.

Deposition of gold on BaTNT changed its acid-base properties. With increasing Au content, the basicity of the catalyst decreased while its acidity increased. In this set of catalysts, it is not correct to correlate styrene conversion with acidity/basicity as the size and content of Au are also changing. However, one can make correlations between turnover frequency (TOF) and acid/base site density. Fig. 6 demonstrates that the intrinsic catalytic activity of supported Au nanoparticles (TOF) for styrene oxidation with TBHP (5.5 M, in decane) increases with increasing basic sites density while an inverse relationship prevails with the acid sites density. Except for Au(0.5 wt.%)/BaTNT, a similar relation was found also between SO selectivity and base/acid sites density. In other words, the acid-base properties of the support influence the catalytic activity of supported Au nanoparticles. A similar observation of increase in catalytic activity of gold with increasing basicity was reported also by Yin et al. [15] and Huang et al. [45] for Au on Al₂O₃ and Patil et al. [42] for Au on Group IIIa metal (Al, Ga, In and Tl) oxides. Basic sites control the particle size of Au [25], facilitate hydrogen abstraction and activation of oxidant molecules, weaken the O–O bond of the chemisorbed reactive oxygen species and thereby, enhance the oxidation activity of supported Au nanoparticles.

3.2.2. In situ spectral characterization, reactive oxo species and reaction mechanism

DRUV-vis and FT-Raman spectroscopic techniques were used to monitor the reactive oxygen species (ROS) generated on BaTNT and Au/BaTNT surfaces during oxidation reactions (Figs. 7 and 8). Known quantities of dried BaTNT and Au(2 wt.%)/BaTNT were contacted with a known quantity of solvent (H₂O or ACN), oxidant (aq. H₂O₂, or TBHP in decane) and substrate (styrene) and the spectra were recorded. “Neat” BaTNT showed three overlapping O → Ti(IV) charge transfer bands at 203, 228 and 272 nm (Fig. 7(i); trace (a)). These have been corresponded to defect unsaturated (tetra- and penta-coordinated) and saturated (hexa-coordinated) Ti sites in titanate nanotubes, respectively [38,46]. Intensity of the UV bands increased on contacting BaTNT with H₂O or ACN (Fig. 7(i), traces (b) and (d)). On treating with aq. H₂O₂, an isosbestic point at 313 nm and a new broad band at 360 nm were detected (Fig. 7(i), traces (c) and (e)) indicating the formation of a new species. The colour of the sample changed to yellow. Similar observation was found also when BaTNT was treated with TBHP in decane (Fig. 7(i), trace (f)). The new band emerged as a consequence of interaction of peroxides (H₂O₂ and TBHP) with Ti⁴⁺ centres is attributed to the formation of “Ti-oxo” species. This band is a charge transfer transition from hydroperoxide(HOO⁻)/alkylperoxide(ROO⁻) to Ti⁴⁺ [37,38]. Similar observations were found also when Au(2 wt.%)/BaTNT instead of BaTNT was used in the study (Fig. 7(ii)). The supported Au catalysts showed additionally the LSPR band at 580 nm. Intensity of this band changed with the addition of solvent, oxidant and substrate due to change in the dielectric constant of the medium. On contact with styrene, the new band due to “Ti-oxo” species at 360 nm diminished evidencing its reactivity with the epoxide molecule. In other words, this study reveals that hydroperoxy/alkylperoxy-Ti/Au are the reactive oxygen species generated during the epoxidation reaction. While no separate band due to “Au-oxo” species was detected, it is likely that this band must have overlapped with the “Ti-oxo” band or spillover of hydroperoxy/alkylperoxy ions from Au to Ti and vice versa is possible. There was some increase in the intensity of ROS band at 360 nm when Au was present on BaTNT. In other words, Au facilitated the formation of ROS species.

Raman spectroscopy is a sensitive and specific technique capable of identifying various oxo intermediates (peroxy and superoxo) generated during oxidation reactions. Fig. 8 shows representative FT-Raman spectra of BaTNT and Au(1 wt.%)/BaTNT contacted with ACN and H₂O₂/TBHP. An intense band at 877 cm⁻¹ corresponding to peroxy species [47] was observed for BaTNT and Au(1 wt.%)/BaTNT when contacted with ACN+ H₂O₂. This was absent in the spectra of “neat” BaTNT and Au/BaTNT (Fig. 3(ii)). Intensity of this band at

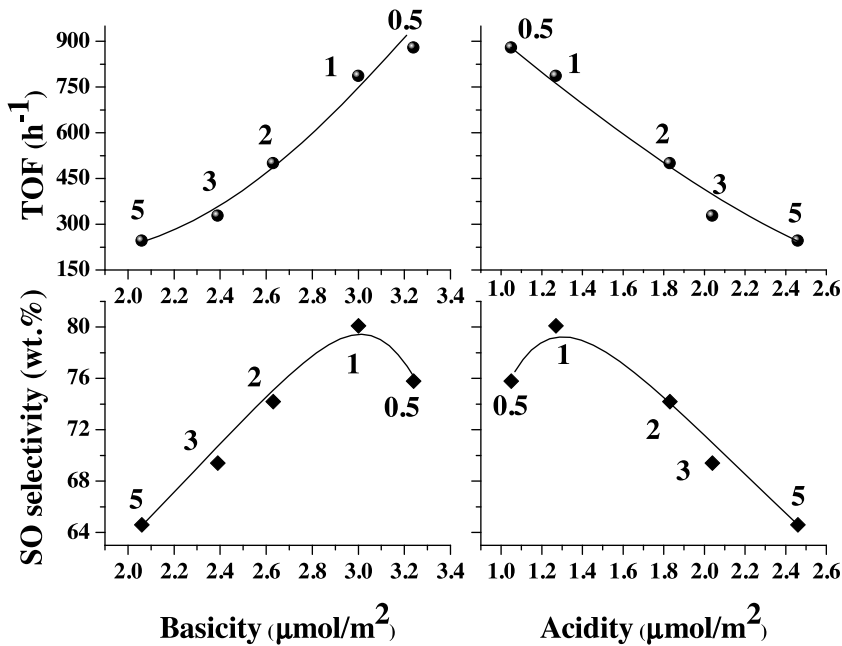


Fig. 6. Correlation between catalytic oxidation activity (TOF and SO selectivity) and acid/base site density of Au/BaTNT catalysts. Numbers on the curves represent Au loading (wt.%) on BaTNT. Reaction conditions: same as in Table 2.

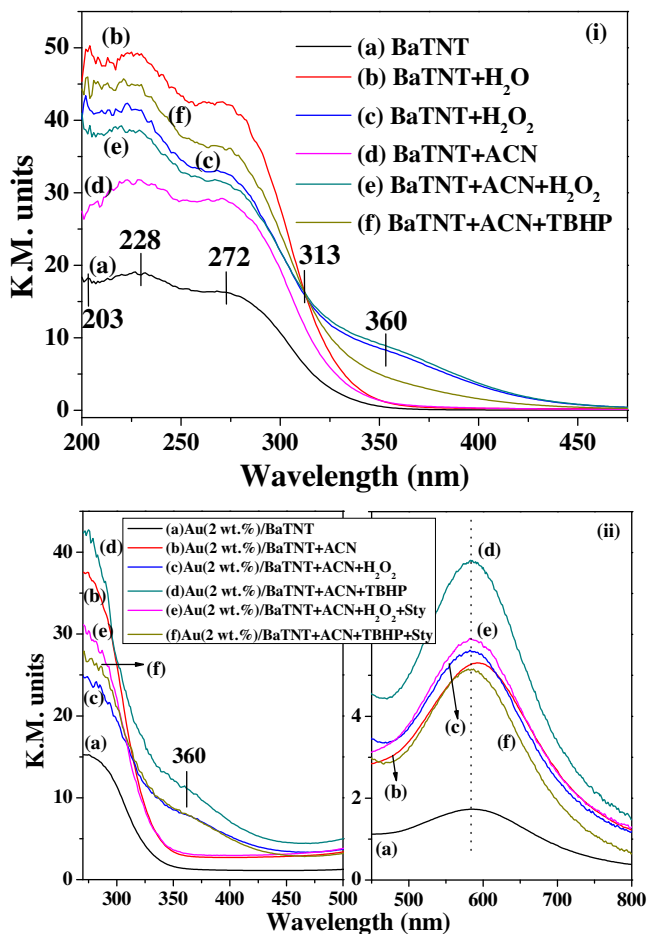


Fig. 7. DRUV-vis spectra of (i) BaTNT and (ii) Au(2 wt. %)/BaTNT treated with solvent (H_2O /acetonitrile-ACN), oxidant (H_2O_2 /TBHP) and styrene (Sty.).

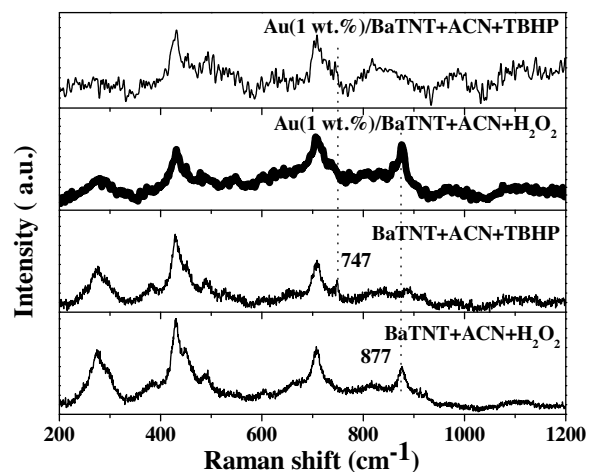


Fig. 8. FT-Raman spectra of BaTNT and Au(1 wt. %)/BaTNT treated with acetonitrile (ACN) and oxidant (H_2O_2 /TBHP).

877 cm^{-1} was higher for Au(1 wt. %)/BaTNT + ACN + H_2O_2 than for BaTNT + ACN + H_2O_2 indicating that Au nanoparticles enhance the formation of *reactive oxygen species*. The position of this band for *reactive peroxy species* shifted to lower wave numbers (747 cm^{-1}) when the materials were contacted with TBHP instead of H_2O_2 . Chan et al. [48] assigned this band at 747 cm^{-1} to stretching vibrations of alkylperoxy species. Low conversion of styrene (1.0%) with molecular oxygen as oxidant (Table 2) suggests that the supported Au in Au(1 wt. %)/BaTNT is not able to generate the right kind of *reactive oxygen species* required for epoxidation. This could also be due to the larger size of Au particles (5.2 nm) in the present catalysts than the threshold limitation of 3 nm required for oxygen activation [4].

A tentative reaction mechanism for oxidation of styrene with peroxides over Au/BaTNT is shown in Fig. 9. Many researchers have addressed the reaction path of styrene oxidation on gold surfaces [2,39,49]. When peroxides like H_2O_2 or TBHP interact with

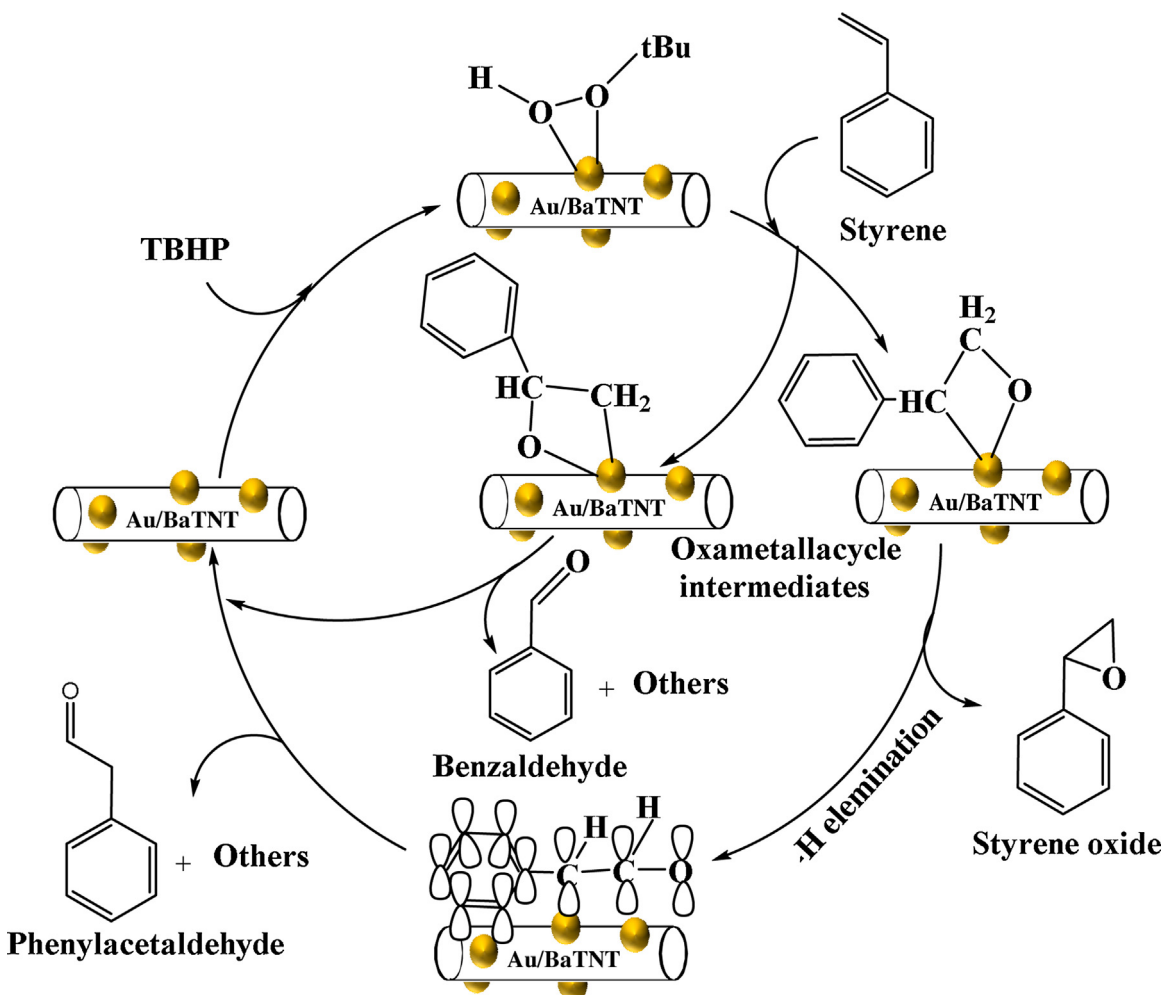


Fig. 9. Possible mechanism for styrene oxidation over Au/BaTNT catalysts.

active Au or Ti^{4+} , a metal-hydro/alkylperoxy species is formed. These peroxy species have been identified by DRUV-vis and FT-Raman spectroscopies (Figs. 7 and 8). These species by undergoing one electron reduction and loss of water molecule form Au-oxo species [4]. The first step in epoxidation is the addition of oxygen to the terminal double bond. Two kinds of intermediate oxametallacycles are formed in the case of styrene. Further conversion of oxametallacyclic species into products is considered as the rate determining step [2,49], wherein epoxide is obtained from a metalloepoxy intermediate through transfer of oxygen to the olefinic bond and benzaldehyde from the breakage of the C–C bond. β -Hydride elimination from the oxametallacyclic species forms phenylacetaldehyde [50]. While the reactive oxygen species formed in the reactions with H_2O_2 and TBHP have been identified as hydroperoxide and alkylperoxide species of Au/Ti, FT-Raman spectroscopy showing characteristics bands at 877 and 747 cm^{-1} for these species lends information that the O–O of peroxide is weaker in the case of Au/Ti-alkylperoxide (formed by using TBHP) than in Au/Ti-hydroperoxide (formed by using H_2O_2). The alkyl group due to its positive inductive effect enhances electron density in oxygen π^* orbitals and thereby leads to weakening of the O–O bond. In other words, formation of Au-oxo species (discussed in the oxidation mechanism) is more facile with TBHP than with H_2O_2 oxidant. Thus, styrene conversion was higher while using TBHP than with H_2O_2 .

4. Conclusions

Gold nanoparticles supported on BaTNT exhibited high catalytic activity for selective oxidation of styrene with molecular oxygen, ($H_2 + O_2$), H_2O_2 and TBHP. Gold loading (0.5–5 wt.%) and oxidant type showed marked effect on styrene conversion and epoxide selectivity. At optimized conditions, epoxide selectivity as high as 80.1 wt.% at a styrene conversion of 60.5 wt.% was obtained over Au(1 wt.%)/BaTNT while using TBHP (in decane, 5.5 M) as oxidant. The catalytic performance of these catalysts is comparable or somewhat higher than the known catalysts. Au/BaTNT are recyclable with little loss in catalytic performance and structural stability. These catalysts were active in oxidations even at 40°C and atmospheric pressure. They activate molecular oxygen and hydrogen producing hydrogen peroxide *in situ* for its further use in styrene oxidation. The transient reactive oxygen species generated during oxidation reactions were followed by *in situ* DRUV-vis and FT-Raman spectroscopy. A tentative reaction mechanism involving these peroxy species was proposed.

Acknowledgment

D.N. acknowledges Council of Scientific and Industrial Research (CSIR), New Delhi for the award of research fellowship.

Appendix A. Supplementary data

Supplementary data associated with this article can be found, in the online version, at <http://dx.doi.org/10.1016/j.apcata.2016.05.014>.

References

- [1] Kirk-Othmer Encyclopedia of Chemical Technology, Vol. 9, 4th Ed., J. Wiley & Sons New York, 1994, p. 915.
- [2] X. Deng, C. Friend, *J. Am. Chem. Soc.* 127 (2005) 17178–17179.
- [3] A.S.K. Hashmi, G.J. Hutchings, *Angew. Chem. Int. Ed.* 45 (2006) 7896–7936.
- [4] M. Turner, V.B. Golovko, O.P.H. Vaughan, P. Abdulkin, A.B. Murcia, M.S. Tikhov, B.F.G. Johnson, R.M. Lambert, *Nature* 454 (2008) 981–984.
- [5] V.R. Choudhary, D.K. Dumbre, N.S. Patil, B.S. Upadhe, S.K. Bhargava, *J. Catal.* 300 (2013) 217–224.
- [6] I. Nongwe, V. Ravat, R. Meijboom, N.J. Coville, *Appl. Catal. A: Gen.* 466 (2013) 1–8.
- [7] J. Huang, M. Haruta, in: Bridging Heterogeneous and Homogeneous Catalysis: Concepts, Strategies and Applications, L. Can, L. Yan (Eds.), Wiley-VCH Verlag GmbH & Co. KGaA, 2014, Ch. 11, pp. 397–424.
- [8] M. Haruta, *Catal. Today* 36 (1997) 153–166.
- [9] T. Hayashi, K. Tanaka, M. Haruta, *J. Catal.* 178 (1998) 566–575.
- [10] Y. Zhu, H. Qian, M. Zhu, R. Jin, *Adv. Mater.* 22 (2010) 1915–1920.
- [11] Y. Yao, X. Zhang, J. Peng, Q. Yang, *Chem. Commun.* 51 (2015) 3750–3753.
- [12] V.R. Choudhary, R. Jha, P. Jana, *Green Chem.* 8 (2006) 689–690.
- [13] N.S. Patil, B.S. Upadhe, D.G. McCulloh, S.K. Bhargava, V.R. Choudhary, *Catal. Commun.* 5 (2004) 681–685.
- [14] N.S. Patil, B.S. Upadhe, P. Jana, S.K. Bharagava, V.R. Choudhary, *J. Catal.* 223 (2004) 236–239.
- [15] D. Yin, L. Qin, J. Liu, C. Li, Y. Jin, *J. Mol. Catal. A: Chem.* 240 (2005) 40–48.
- [16] F. Zhang, X. Zhao, C. Feng, B. Li, T. Chen, W. Lu, X. Lei, S. Xu, *ACS Catal.* 1 (2011) 232–237.
- [17] Y. Liu, H. Tsunoyama, T. Akita, T. Tsukuda, *Chem. Commun.* 46 (2010) 550–552.
- [18] N. Linares, C.P. Canlas, J. Garcia-Martinez, T.J. Pinnavaia, *Catal. Commun.* 44 (2014) 50–53.
- [19] Y. Jin, D. Zhuang, N. Yu, H. Zhao, Y. Ding, L. Qin, J. Liu, D. Yin, H. Qin, Z. Fu, D. Yin, *Microporous Mesoporous Mater.* 126 (2009) 159–165.
- [20] J. Jiang, Q. Gao, Z. Chen, *J. Mol. Catal. A: Chem.* 280 (2008) 233–239.
- [21] M. Toth, J. Kiss, A. Oszko, G. Potari, B. Laszlo, A. Erdohelyi, *Top. Catal.* 55 (2012) 747–756.
- [22] V. Idakiev, Z.-Y. Yuan, T. Tabakova, B.-L. Su, *Appl. Catal. A: Gen.* 281 (2005) 149–155.
- [23] T. Murciano, Q. He, G.J. Hutchings, C.J. Kiely, D. Chadwick, *ChemCatChem* 6 (2014) 2531–2534.
- [24] D. Nepak, D. Srinivas, *Catal. Commun.* 58 (2015) 149–153.
- [25] D. Nepak, D. Srinivas, *RSC Adv.* 5 (2015) 47740–47748.
- [26] T. Kasuga, M. Hiramatsu, A. Hoson, T. Sekino, K. Niihara, *Langmuir* 114 (1998) 3160–3163.
- [27] R. Si, M.F. Stephanopoulos, *Angew. Chem. Int. Ed.* 47 (2008) 2884–2887.
- [28] P. Pusztai, R. Puskás, E. Varga, A. Erdohelyi, Á. Kukovecz, Z. Kónya, J. Kiss, *Phys. Chem. Chem. Phys.* 16 (2014) 26786–26797.
- [29] Y. Wen, B. Liu, W. Zenga, Y. Wang, *Nanoscale* 5 (2013) 9739–9746.
- [30] D.V. Bavykin, M. Caravetta, A.N. Kulak, F.C. Walsh, *Chem. Mater.* 22 (2010) 2458–2465.
- [31] T. Gao, H. Fjellvag, P. Norby, *Inorg. Chem.* 48 (2009) 1423–1432.
- [32] D. Yang, H. Liu, L. Liu, S. Sarina, Z. Zheng, H. Zhu, *Nanoscale* 5 (2013) 11011–11018.
- [33] B. Puertolas, A.K. Hill, T. Garcia, B. Solsona, L. Torrento-Murciano, *Catal. Today* 248 (2013) 115–127.
- [34] M. Teranishi, S.-i. Naya, H. Tada, *J. Am. Chem. Soc.* 132 (2010) 7850–7851.
- [35] L. Torrente-Murciano, Q. He, G.J. Hutchings, C.J. Kiely, D. Chadwick, *ChemCatChem* 6 (2014) 2531–2534.
- [36] L. Torrente-Murciano, T. Villager, D. Chadwick, *ChemCatChem* 7 (2015) 925–927.
- [37] Y. Zhu, H. Qian, R. Jin, *Chem. Eur. J.* 16 (2010) 11455–11462.
- [38] V.N. Shetti, P. Manikandan, D. Srinivas, P. Ratnasamy, *J. Catal.* 216 (2003) 461–467.
- [39] Z. Opire, T. Mallat, A. Baiker, *J. Catal.* 245 (2007) 482–486.
- [40] J. Liu, F. Wang, T. Xu, Z. Gu, *Catal. Lett.* 134 (2010) 51–55.
- [41] J. Liu, F. Wang, T. Xu, Z. Gu, *Catal. Lett.* 134 (2010) 51–55.
- [42] N.S. Patil, R. Jha, B.S. Upadhe, S.K. Bhargava, V.R. Choudhary, *Appl. Catal. A: Gen.* 275 (2004) 87–93.
- [43] J. Liu, F. Wang, S. Qi, Z. Gu, G. Wu, *New J. Chem.* 37 (2013) 769–774.
- [44] P. Huang, G. Chen, Z. Jiang, R. Jin, Y. Zhu, Y. Sun, *Nanoscale* 5 (2013) 3668–3672.
- [45] J. Huang, Y. Wang, J. Zheng, W.-L. Dai, K. Fan, *Appl. Catal. B: Environ.* 103 (2011) 343–350.
- [46] B. Chowdhury, J.J. Bravo-Suarez, N. Mimura, J. Lu, K.K. Bando, S. Tsubota, M. Haruta, *J. Phys. Chem. B* 110 (2006) 22995–22999.
- [47] P. Lakshmanan, F. Averseng, N. Bion, L. Delannoy, J.-M. Tatibouet, C. Louis, *Gold Bull.* 46 (2013) 233–242.
- [48] H.-Y. Chan, V.-H. Nguyen, J.C.S. Wu, V.C. Casilda, M.A. Banares, H. Bai, *Catalysts* 5 (2015) 518–533.
- [49] R. Quiler, X. Liu, C. Friend, *Chem.: Asian J.* 5 (2010) 78–86.
- [50] L. Zhou, R. Madix, *J. Phys. Chem. C* 112 (2008) 4725–4734.